Received: 25 July 2022 | Revised: 7 December 2022 | Accepted: 7 December 2022

DOI: 10.1002/ppap.202200136

RESEARCH ARTICLE

PLASMA PROCESSES AND POLYMERS

Electrochemical impedance spectroscopy evaluation of nonthermal plasma restoration for ductile metals in cultural heritage artifacts

Patricia Giménez-Barrera[1,2] | **Sergi Colominas**[2] | **Salvador Borrós**[1]

[1]Grup d'Enginyeria de Materials (GEMAT), Barcelona, Spain

[2]Grup de Química Analítica, Institut Químic de Sarrià, Universitat Ramon Llull, Barcelona, Spain

Correspondence
Salvador Borrós, Grup d'Enginyeria de Materials (GEMAT), Barcelona, Spain.
Email: salvador.borros@iqs.url.edu

Abstract

Despite the large number of studies devoted to understanding the degradation process of ductile metals in cultural heritage, there is still a lack of consolidated protocols for their restoration. Traditional restorations such as chemical cleaning and electrochemical treatments are carried out for the recovery of corroded ductile metals. However, these techniques are usually very aggressive to the metallic surface. For this reason, a cold plasma design is presented to restore ductile metals through the minimum intervention criterion. Lead samples were induced to atmospheric acetic acid corrosion to recreate models of degradation for practical restoration and characterization. The material after plasma treatment was analyzed with different techniques of characterization, including electrochemical impedance spectroscopy. The present work demonstrated the potential of this technique to provide an accurate analysis of its surface.

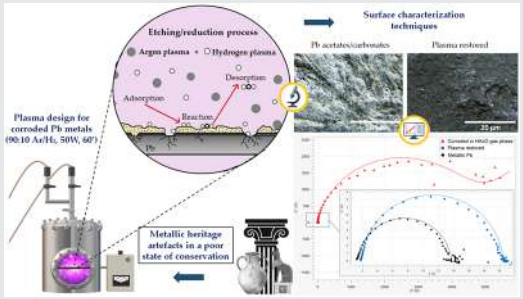

KEYWORDS

acetic acid corrosion, cold plasma, electrochemical impedance spectroscopy, lead corrosion, restoration

1 | INTRODUCTION

Thanks to their physical characteristics, such as malleability, ductile metals had a great attraction for the creation of numerous artistic, architectural, and technical purposes. Ductile metals have a higher degree of plastic deformation in contrast to other metals, which increases the facility to shape different forms and makes it easy to manipulate.[1] Due to these properties, ductile metals have been used in a great number of artifacts that

provide useful information about our history and conform to the metallic Cultural Heritage. In ancient times, the malleable properties of ductile metals were commonly associated with the creation of utensils, coins, medals, and plates, where inscriptions were engraved. In the artistic field, *embossing* is the most common technique for decorating objects, where it takes advantage of its malleability to obtain a particular engraving.[2]

The main problem in the metallic field is the instability of the collections and their long-term conservation under the effects of the corrosion phenomenon. In this context, corrosion is a serious problem that not only chemically affects ductile metals but also structurally, producing embrittlement and physical changes that can affect the original form. As a result, these metals are difficult to conserve since they are generally susceptible to deformation.

Lead belongs to different archaeological and artistic objects, documented as one of the first metal castings. Corrosion on metallic lead was reported as early as 1921.[3] Specifically, lead degradation under organic acid atmospheres is considered a challenge for many restorers. This is the most aggressive chemical since corrosion products are easily soluble and can dissolve part of the metallic structure. In this sense, it is known that certain species of wood are very aggressive to lead because of the breakdown of cellulose compounds in the timber, and it produces volatile organic compounds (VOCs), especially acetic acid.[4,5] The effect of VOCs on lead corrosion is significant in the context not only of buildings but also in museums for the display of historic artifacts. The origin of this degradation is localized in the form of pitting corrosion and ends with the creation of a lead carbonate layer expanded through the surface.[6] The structural composition of the formed corrosion products is reported in different studies,[7,8] mainly in the form of cerussite and plumbonacrite.

During the fifties, chemical cleanings such as the *Caley method*,[9] were applied by conservators to eliminate the corrosion products on lead artifacts. However, these treatments were usually aggressive chemicals that ended up causing a double problem over time; physical effects such as embrittlement, erosion, or deformation, and chemical effects with the introduction of new elements from the liquid solution used during the treatment, which can create new corrosion products once again over time. In 1956, Plendereith promoted the use of electrochemical methods, which had its apex until nowadays in the metallic restoration field.[10] However, the consequences of electrochemical treatments were directly reflected in the low innocuousness of the technique. The immersion of the sample in an electrolyte, puts the structure at risk of damage, causing changes in its properties by the introduction of the fragile state object into a liquid medium. In this context, the concept of *innocuousness* is important to preserve the integrity of the artifacts to restore, and this practice must be performed within the minimum intervention criterion. This point of view suggests a change of the traditional techniques to new methodologies.

For this reason, in recent years, less invasive restoration techniques have been developed and cold plasma is in the front line of these techniques.[11–13] In the present study, a non-thermal plasma reactor, designed by *Grup d'Enginyeria de Materials* (GEMAT) at IQS (*Universitat Ramon Llull)*.[14–16] was used to restore corroded lead samples under an argon/hydrogen plasma. In previous studies,[12–15] it was reported that the plasma reactor was a useful tool to restore corroded surfaces from Cultural Heritage artifacts question, to solve after applying any restoration method, is to assure the integrity of the treated surface. For this reason, it is important to develop, in parallel to the restoration ones, characterization techniques that give insight into the artifact evolution during cleaning. In this sense, electrochemical impedance spectroscopy (EIS) is a technique that has been used for over a century and 30 years to fine-characterize the surface evolution in corroded samples.[17–27] It was proposed in this work to use EIS to analyze how corroded surfaces can variate before and after cold plasma treatment in studied lead samples. EIS analysis was complemented by different surface characterization techniques such as X-ray photoelectron spectroscopy (XPS), X-ray diffraction (XRD), scanning electron microscopy/energy dispersive spectroscopy (SEM-EDS), and confocal microscope.

In this work, a non-Thermal Plasma treatment to restore lead artifacts was developed. This treatment could avoid the use of other aggressive techniques and prevent damage to the metallic surface. Lead samples have been induced to atmospheric acetic acid corrosion, to recreate models of degradation for practical restoration and characterization analysis. To understand the restoration process, it has been tuned up different characterization techniques of the restored samples, especially EIS. This technique has demonstrated the potential to provide a fairly accurate analysis of its surface and it is presented as a useful and complementary tool to the classic techniques for surface analysis.

2 | MATERIALS AND METHODS

2.1 | Plasma reduction

A low-pressure plasma reactor was used for restoring metallic lead samples corroded by acidic environments. The experimental setup was designed by *Grup d'Enginyeria de Materials* (GEMAT) at IQS (*Universitat Ramon Llull)* and previously reported in other papers.[14–16] The schematic system of the plasma reactor used is presented in Figure 1.

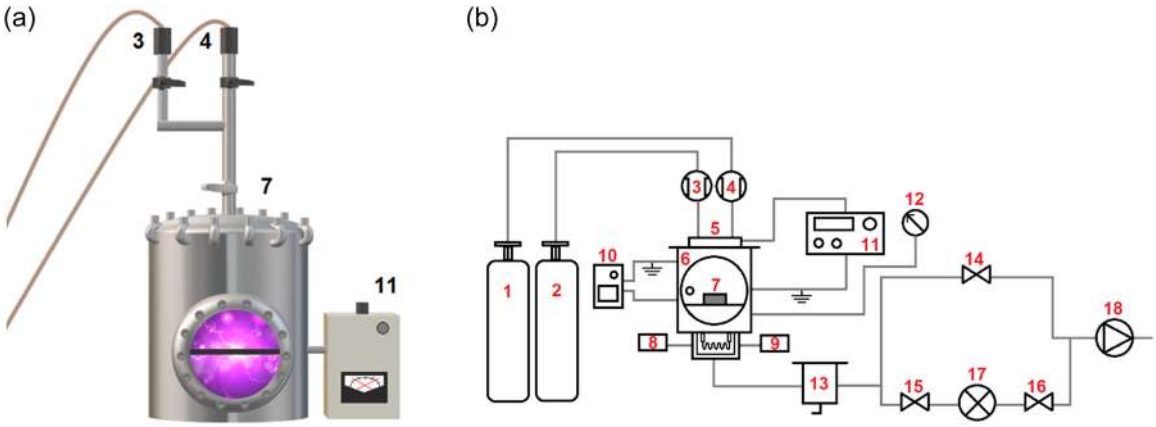

FIGURE 1 (a) Low-pressure plasma reactor and (b) schematic drawing of the experimental set-up; 1, 2—hydrogen, argon; 3, 4—mass flow controllers; 5—gas inlet and mixing; 6—reactor chamber; 7—sample; 8, 9—thermocouples; 10, 11—RF power supply and matching network; 12—capacitance pressure gauge; 13—chemical inlet trap (carbon active); 14, 15, 16—valves; 17—refrigerated inlet trap (dry ice); 18—vacuum pump.

Briefly, the reactor has a Bell Jar design with a stainless-steel chamber (diameter, 25.5 cm; length, 41.6 cm). The ground electrode is the reactor chamber, and the radio frequency (RF) electrode is an aluminum plate, which also is used to hold the samples. Additionally, the RF electrode is connected to an RF pulse generator (13.56 MHz) via a matching box.[28–30] Gases were injected into the system via a standard manifold. Gas fluxes were adjusted by two mass flow controllers (elements 3 and 4), and two ball valves were used to cut the gas flux, if needed, in the reactor chamber. The system pressure is monitored using a vacuum gauge controller (MKS PDR900) connected with a cold cathode/micropirani vacuum transducer (MKS 972 DualMag) positioned at the center of the reactor. The system used a rotary vane vacuum pump (Trivac D 16BCS/PFPE Leybold). Also, it has a nitrogen cold trap and a chemical trap filled with active carbon to protect the vacuum pump from the condensed vapors. The typical base pressure for all experiments is close to 0.06 Pa, and Ar/H_2 gases were introduced at a constant pressure of ~10 Pa.

Before the introduction of the samples placed on an aluminum plate, the chamber was cleaned in continuous wave argon/hydrogen (2:1) plasma for approximately 1800 s at a power of 50 W. To optimize the study, a full factorial design was used. In this study, different conditions (time, power, and argon-hydrogen ratio) were chosen to determine the capacity of reducing corrosion in Pb samples.

To evaluate the effectiveness of plasma restoration on corroded Pb samples (99.77%, Amat Metalplast SA), a set of eight polished lead samples was used. All samples were previously polished with SiC paper (GRIT 800, 1200, 2000, and 4000 supplied by Struers). Then, they were chemically corroded by acetic acid for 1 week, following the procedure explained in Section 2.3. In this case, as it was mentioned in Section 2.1, a mixture of argon and hydrogen was selected for the cold plasma. The base pressure was 0.06 Pa. Then, argon and hydrogen gases were injected until reaching a working pressure (P_p) of approximately 10 Pa. When the working pressure was reached, the generator was turned on, and the gas in the chamber of the plasma was initiated. The vacuum chamber continuously received gas, so a continuous renewal of the gases was produced inside the chamber.

To optimize the cold plasma treatment, a full factorial experimental design for corroded metallic Pb was performed. To classify the results in a normalized scale, five features were selected: treatment time (min) (A), plasma power (W) (B), and Ar/H_2 ratio (C). Pressure could be a factor to be considered, but it was decided to perform all experiments at 0.06 Pa.

2.2 | Preparation of working electrodes for electrochemical measurements

The working electrode preparation consisted of the insertion of a 99.999% Pb rod (Sigma-Aldrich) into a PTFE holder. Lead cylinders were introduced into a 6.35 mm diameter cavity on the PTFE holder, of 15 mm of thickness in total. Then, the surface of the working electrode was initially prepared by mechanical polishing with SiC polishing paper (supplied by Struers) with successive decreasing the grain size; GRIT 800−1200−2000−4000. The working lead electrode was used in an RDE (rotating disk electrode) system to be

rotated at 1500 rpm during polarization. Electrical contact with the lead working electrode was provided using an internal disk contact with a spring-loaded probe.

EIS measurements were performed using a Metrohm Autolab PGSTAT 302 N. The assembly was prepared with a three-electrode setup connected to the data acquisition equipment. EIS measurements were performed, after 1 h of stabilization time,[31] using a signal amplitude of 10 mV versus the open circuit potential and the frequency range from 1E + 05 to 0.1 Hz. Ten points of frequency per decade were collected. The experimental conditions were chosen according to the bibliography.[31–33] Data modeling was performed using Nova 2.1 Software. Oxygen in the electrolyte was displaced by sparing nitrogen one-hour before the measurements.

2.3 | Accelerated corrosion in lead samples

Lead electrodes were anodized in 5 M H_2SO_4 to generate an accelerated corrosion layer on the electrode surface. Anodization was performed at 0.8 V versus Ag/AgCl/KCl (3 M) reference electrode for 1800 s. The applied potential was chosen according to the bibliography to form a stable passive layer.[34–37] Anodization was performed using a 3-electrode setup and a potentiostat/galvanostat Autolab PGSTAT 302 N.

On the other hand, a different set of samples was chemically corroded using acetic acid. Specimens were corroded by wetting the metal surface with 100 μl of glacial acetic acid that covered the entire metal surface (1.26 cm^{-2}). After 1 h, the surface was dried (without washing) using a hot stream of air. Samples were prepared by repeating that procedure three times a day for 1 week and stored in the lab after preparation (at room temperature and exposed to air).

2.4 | Samples analyses

XRD analysis was performed with an X'Pert PANalytical Diffractometer using CuKα radiation in the Bragg-Brentano on the surface of the treated lead. A continuous scan mode was used to collect 2θ data from 10° to 80° with a 0.013 sampling pitch at a scan rate of 3 min^{-1}. Crystalline phases were identified by X'Pert Highscore software. The intensities of the standard sample were retrieved from the PDF-2 database (ICDD®).

Once samples were electrochemically reduced or plasma treated, they were analyzed with XPS in PHI 5500 multitechnique system from physical electronics, with a monochromatic X-ray source. The selected resolution for the spectra of the different elements in the depth profile spectra was 23.50 eV of Pass Energy and 0.25 eV/step. The high-resolution spectra were obtained through a grade of penetration of 5 nm and the depth profile was of the order of 50 nm. The resulting spectra were analyzed and deconvoluted with the Multipak Version 5.0A software. XPS measurements on samples before and after cold plasma treatment were completed with a delay of 1 day. During this time interval, samples were stored in hermetic polypropylene sample containers (50 ml), purged, and filled with argon to remove air.

All samples, before and after being treated, were characterized using a JEOL JSM-5310 scanning electron microscope coupled with an Oxford Inca Energy 200 EDS system.

3 | RESULTS AND DISCUSSION

3.1 | Cold plasma treatment on corroded lead samples

Corroded lead samples were treated with an argon hydrogen cold plasma as described in Section 2.1. In Figure 2, the proposed mechanism of surface restoration in corroded lead samples is presented.

The plasma treatment of the sample, presented in Figure 2, leads to a physicochemical alteration on the surface. Under these conditions, a large number of energetic reactive species is generated It is important to underline that while hydrogen acts as a reductive treatment, the application of argon in the restoration treatment adds mainly a physical stage.[38] This postulated etching mechanism may involve the removal of lead carbonates and oxides by bombarding the mixture of reactive particles at subsonic velocities.[39–43] A combination of argon and hydrogen plasma increases the effectiveness of the treatment. Ionized argon induces the generation of reactive sites, increasing the efficiency of the hydrogen atoms during plasma reduction.

The effectiveness of this Ar/H_2 plasma can vary substantially depending on the experimental setup. In this way, a full factorial experimental design was performed (see details in Section 2.1). The full factorial design (2^3) proposal is shown in Table 1.

All results were evaluated by a visual characterization to perform an exhaustive analysis of the selected samples. To classify the results in a normalized scale, the finish aspect was defined in five features shown in Table 2. Each feature represents a variable of the non-desired aspect resulting in a cold plasma-treated sample. They were evaluated from 0 to 2 depending

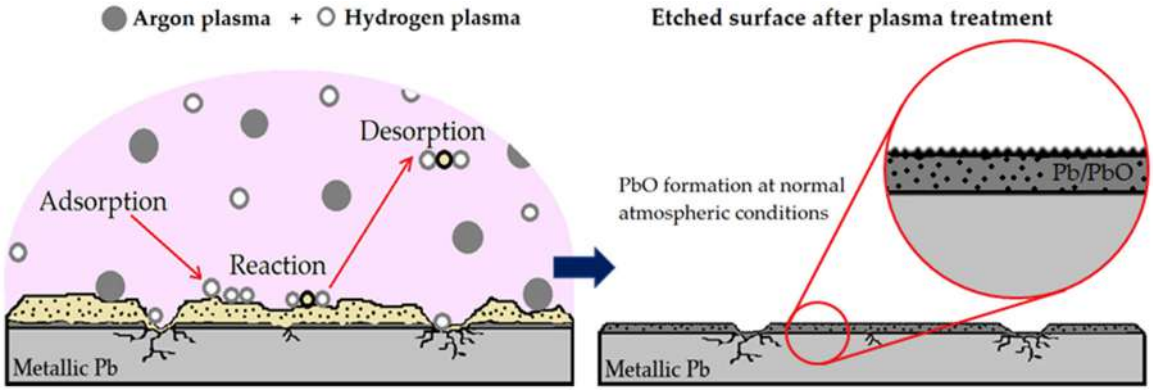

FIGURE 2 Plasma mechanism reactions on a corroded metallic lead (left) and etched surface after plasma treatment (right)

TABLE 1 Full factorial design (2^3) with resulting surfaces

	Factors			Interactions			
Exp.	A Time (min)	B Power (W)	C Ratio	AB	AC	BC	ABC
1	60 (1)	80 (1)	90:10 (1)	1	1	1	1
2	60 (1)	50 (−1)	70:30 (−1)	−1	−1	1	1
3	15 (−1)	80 (1)	70:30 (−1)	−1	1	−1	1
4	15 (−1)	50 (−1)	90:10 (1)	1	−1	−1	1
5	15 (−1)	50 (−1)	70:30 (−1)	1	1	1	−1
6	15 (−1)	80 (1)	90:10 (1)	−1	−1	1	−1
7	60 (1)	50 (−1)	90:10 (1)	−1	1	−1	−1
8	60 (1)	80 (1)	70:30 (−1)	1	−1	−1	−1

TABLE 2 Visual evaluation of resulting samples

	Experiment							
Feature	1	2	3	4	5	6	7	8
Heterogeneity	2	0	2	1	0	2	2	1
Carbonate residues	1	0	1	1	0	2	2	0
Coloration	2	2	2	2	1	2	2	1
Decohesion	1	0	0	2	0	1	2	0
Deformation	2	2	2	2	2	2	2	2
Response (Number of defects)	8	4	7	8	3	9	10	4

on the semiquantitative approach. The higher the value, the better the treatment has been. A value of 2 means the absence of the visual features exposed in Table 2, while 0 is considered a non-desired aspect. The higher the response value, the more desirable the surface aspect was. The influence of each factor is represented as a Pareto chart of factors and a half-normal probability plot shown in Figure 3.

By using visual analysis of the treated surfaces using a numerical evaluation, it was possible to determine the different contributions of the established factors shown in Figure 3. As can be seen, factor C (Ar/H_2 ratio), had the higher influence, as seen in the percentage of contribution (75.46%) in the Pareto Chart of Factors. In addition, in the Half Normal Probability Plot, factor C deviates from the linear trend created by the rest of the points corresponding to the other factors and interactions. Consequently, it is confirmed that factor C is the most important factor. An example of its influence was seen between experiment 1 (ratio of 90:10 argon-hydrogen) and experiment 8 (ratio of 70:30 argon-hydrogen). By fixing the power and time, and varying the ratio, the aspect of the obtained surfaces was quite different (a response value of 8 for experiment 1, and a response of value 4 for experiment 8). With that, it was demonstrated that the etching effect of argon is especially advantageous in terms of extracting corrosion products from the surface. A ratio of 90:10 (Ar/H_2), in combination with a power of 50 W during 3600 s, ensures that the

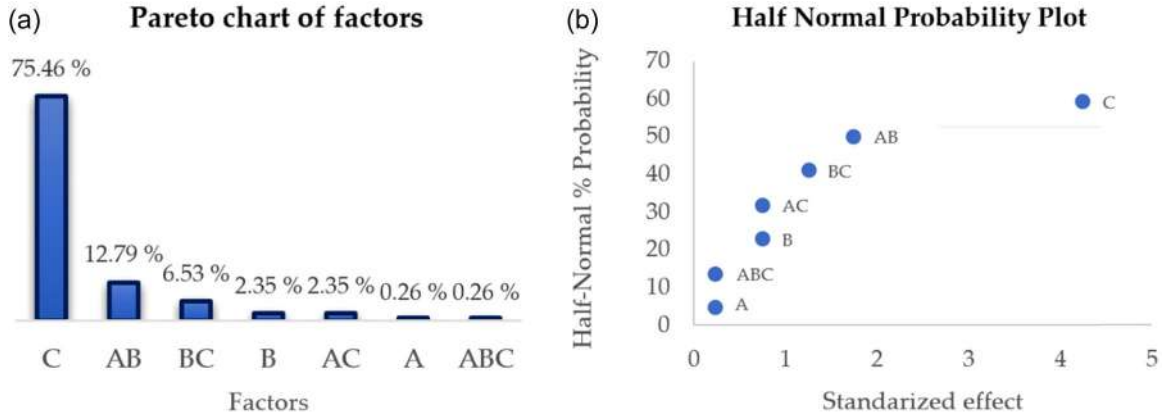

FIGURE 3 (a) Pareto chart of factors graph, (b) half-normal probability plot

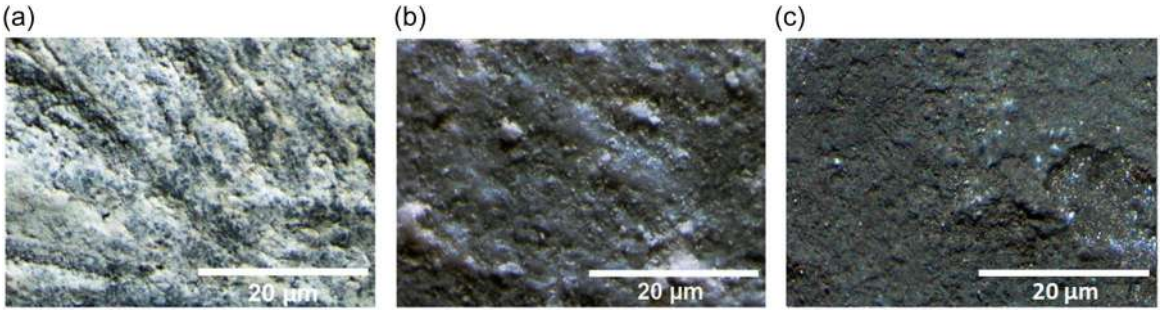

FIGURE 4 (a) Surface aspect of the corroded Pb samples by HAcO gas phase before plasma treatment, (b) surface aspect after plasma treatment of experiment 5 (power applied of 50 W and a ratio of 70:30 argon-hydrogen during 15 min), (c) after plasma treatment experiment 7 (power applied of 50 W and a ratio of 90:10 argon-hydrogen during 60 min).

sample is not overheated, and the treatment can be prolonged, if necessary, without risk of surface damage.

Although the isolated factor of B (power) has a contribution of 2.35% (the same as for the AC interaction), the combination of AB (power with time) increased to a contribution of 12.76%, indicating some synergetic effect between power and time. On the other hand, the BC interaction (power and ratio) was lower (6.53%). In the case of the isolated factor of A (time) and the combination of all factors (ABC), a significant contribution was not seen (both of 0.26%). Finally, it should be commented that at high exposition time (60 min), power (80 W), and argon percentage (90:10 Ar/H_2), superficial damage was observed.

The selected parameters of experiment 7, resulted in a sample with a very good visual appearance. Once it has found which are the key parameters in the development of the plasma restoration method, it was decided to carry out a deeper characterization to confirm the conclusions from the appearance study. The first analysis by SEM-EDX was performed on the sample obtained in the conditions of experiment 7 (long time, low power, and high Ar/H_2 ratio), and the results are shown in the supplementary information (Supporting Information: Figures S1 and S2). The resulting surface was more homogeneous than the nontreated sample, but with a porous aspect due to the etchant effect (contact angle values of 132° for the corroded sample and 67° for the plasma-treated sample). In the EDX analysis, the main elements on the treated sample were lead and a small quantity of oxygen, as also a residual presence of carbon. These results confirm that the plasma treatment on the corroded samples allowed the removal of the carbonated superficial products. Figure 4 shows the corroded surface aspect of the samples before treatment, the resulting treated surface of experiment 5, and the resulting treated surface of experiment 7.

It can be observed in Figure 4 that the sample surface of experiment 5 had corrosion products, and its surface was heterogeneous. In contrast, the surface of experiment 7 was more homogeneous than experiment 5 and no corrosion products on its surface were detected.

To complete the chemical analysis of the cold plasma treatment on corroded Pb metals, XPS was used to

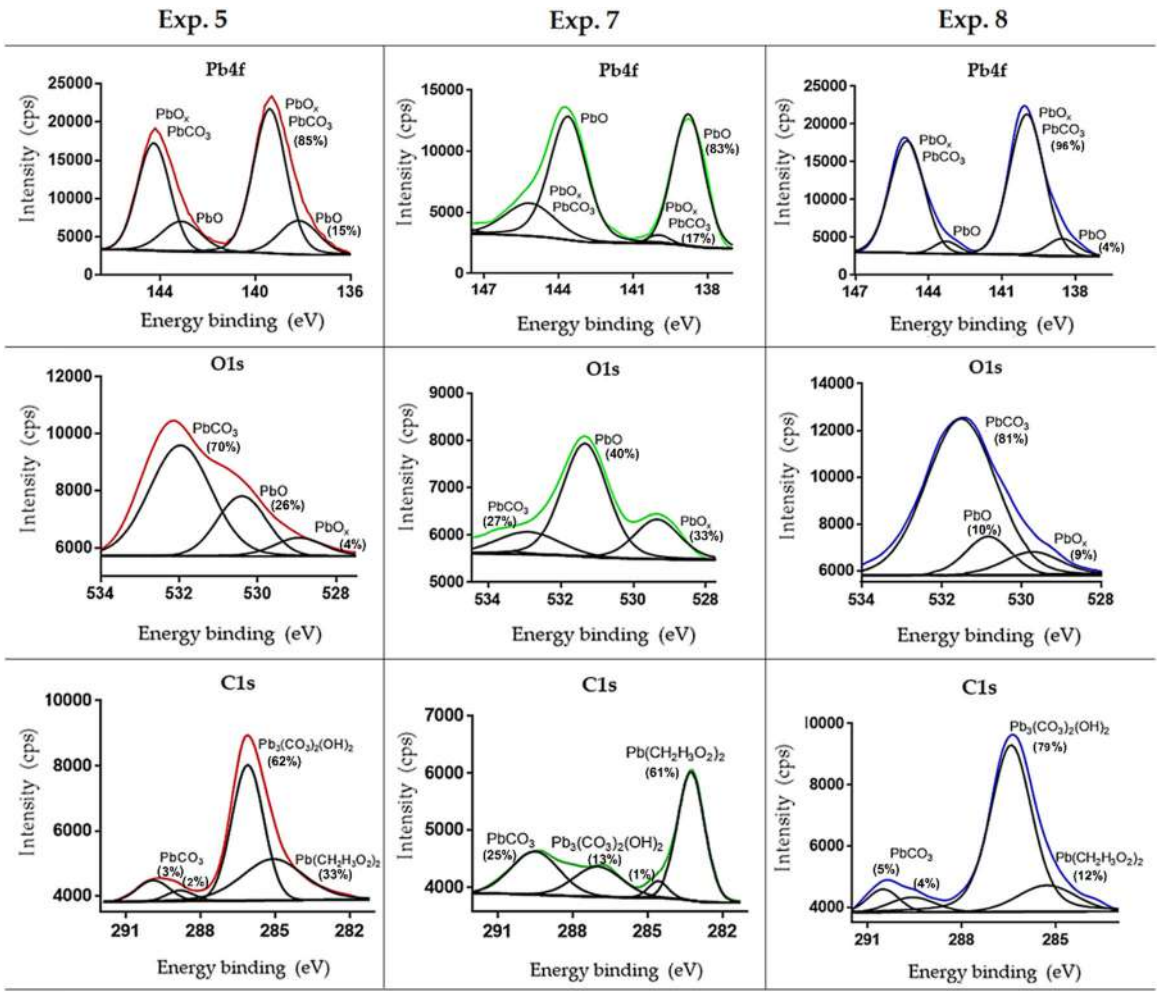

FIGURE 5 High-resolution X-ray photoelectron spectroscope analysis of the selected samples (experiment 5, experiment 7, and experiment 8) for Pbf4 (lead), O1s (oxygen), and C1s (carbon).

identify the chemical state and estimate the electronic structures. XPS can be a good tool to characterize the resulting surfaces and to compare the different superficial compositions, and for this reason, the technique was selected following the reference bibliography found in different databases.[44,45] To perform this analysis, three samples (experiment 5, experiment 7, and experiment 8) were selected to be characterized by XPS to compare their superficial products. Results are shown in Figure 5.

As it was expected, the deconvolutions obtained on the high-resolution results (depth of 5 nm) showed variations, especially in the spectra of experiment 7 compared with experiments 5 and 8. The Pb4f signal of XPS graphs presented in Figure 7, shows clear differences between experiments. In all spectra, a PbO passive layer corresponding to the signal in the 138 eV region was seen. PbO and $PbCO_3$ were associated with the 139.5 eV region. For the O1s spectra in experiments 5 and 8, a lower proportion of lead oxides (PbO/PbO_x) was seen (30% and 19%, respectively). In contrast, a higher proportion of PbO (40%) and PbO_x (33%) were detected in experiment 7. This fact demonstrated that for experiment 7, the residual compounds of lead carbonates were much lower than the other two samples (27%). Lead carbonate products were related to the 285 eV region and associated with cerussite ($PbCO_3$) and hydrocerusite ($Pb_3(CO_3)_2(OH)_2$) formation.[46]

To study the effect of plasma treatment on the internal layers, an XPS depth profile (5 nm/sputtering) of experiment 5, experiment 7, and experiment 8 was performed. The objective was to analyze possible changes between the oxides from the internal layers and the passivation result of each sample. The association of the obtained peaks was done following the previous XPS studies in the Pb4f and O1s region.[34–36,44,45] Results are presented in Figure 6.

As can be seen, different signals for Pbf4 and O1s were shown in the in-depth study. For experiment 7, the innermost layer presented a proportion of 88% of PbO, 4% for PbO_x, and 8% for $PbCO_3$. Moreover, a PbO layer

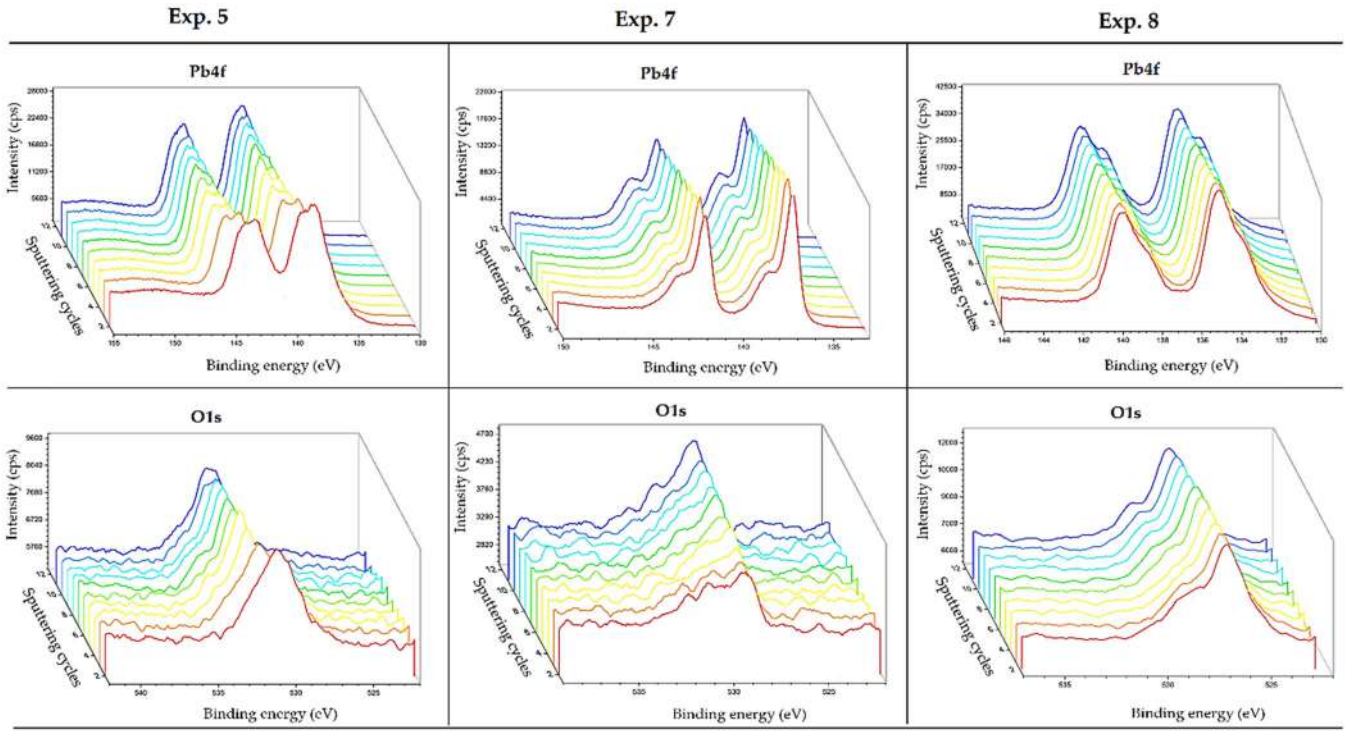

FIGURE 6 Depth profile XPS analysis of experiment 5, experiment 7, and experiment 8 samples for Pbf4 and O1s

(88%) was present in the subjacent layers together with a lower signal in the 532 eV region corresponding to the residual lead carbonate products (8%). These results corroborate the efficacy of argon in the etchant potential of the plasma conditions (90:10 Ar/H_2 experiment 7). In experiment 5, the products assigned to the most internal sputtering (cycle 12) were 50% for $PbCO_3$ (and/or other lead carbonates), 41% to the PbO formation, and 9% to other oxides (PbO_x). For experiment 8, a similar behavior was observed. The PbO_x signal suggests the presence of Pb (II) and Pb (IV), such as PbO_2 or Pb_3O_4 compounds, as can be seen in the 528.9 eV region. Species of this region can be related to lead oxide minerals such as massicot (orthorhombic PbO) or minimum (Pb_3O_4).[37,47] From the XPS results, it can be concluded, that for experiments 5 and 8, the residual corrosion compounds were present in much more quantity than in experiment 7, including the internal layers.

3.2 | Surface analysis of lead samples using EIS

In this section, EIS was used to evaluate the surface characteristics of led samples, after and before their restoration using cold plasma techniques (see Section 2.1.). In an initial experimental campaign, corrosion layers on lead electrodes were prepared. The goal of this campaign was to establish the electrode response using EIS as a function of different corrosive layers, such as lead sulfate and lead acetate. Both layers were generated using the corresponding acids, sulfuric and acetic acid. Note that sulfuric acid produces dense, compact, and well-adhered corrosion layers.[48] In contrast, acetic acid produces voluminous, porous, and partially soluble corrosion products.[49]

In the first set of experiments, a lead electrode was anodized as described in Section 2.2. to generate a lead sulfate corrosion layer on its surface. In this experiment, the sample was anodized at 0.8 V during 1800 s in 5 M H_2SO_4. Anodization potential was chosen according to the bibliography[33,50] to obtain a compact corrosion layer of $PbSO_4$. Immediately after anodization, the electrode impedance was measured. The equivalent circuit was chosen as suggested by different authors [51–53] and it is shown in Supporting Information: Figure S3. In a second experiment, a lead sample was induced to corrode when exposed to vapors of acetic acid for 1 week (as described in see Section 2.2), and then its impedance was measured using 5 M H_2SO_4 as an electrolyte. In that case, due to the variations of the morphology in the corroded surface, a different equivalent circuit was used as suggested in the literature,[31] and it is presented in Supporting Information: Figure S4. Figure 7 shows the impedance measurements obtained for both samples (sulfuric and acetic acid) and the fitting spectra obtained using the proposed

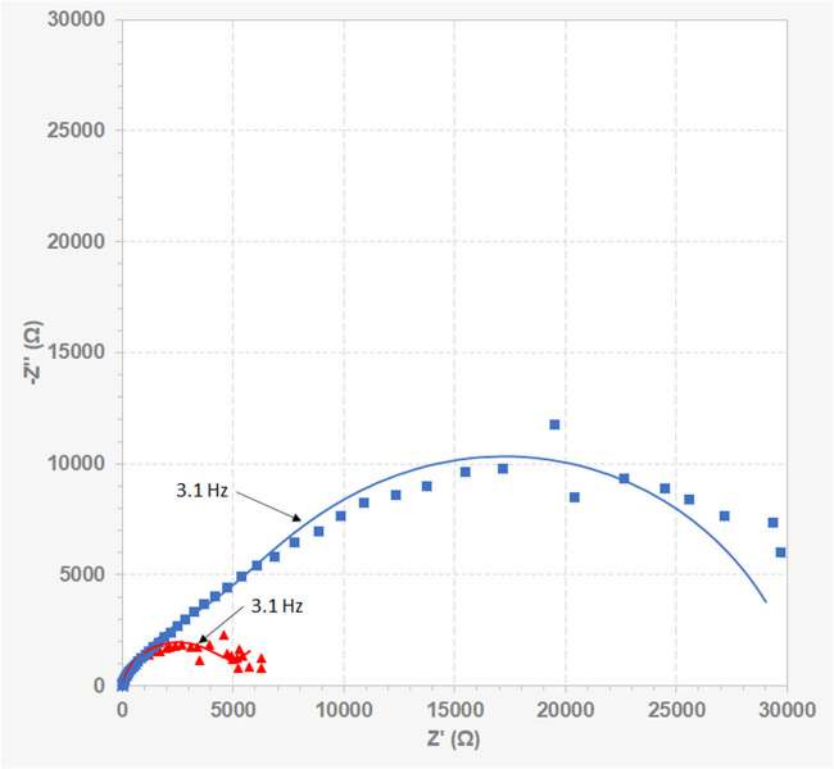

FIGURE 7 Electrochemical impedance spectroscopy spectra of corroded samples, ■ anodized at 0.8 V versus ref during 1800 s in 5 M H_2SO_4 and ▲ exposed at vapors of HAcO for 1 week.

equivalent circuits. Bode plots are shown in Supporting Information: Figures S6 and S7 and data fitting values of both experiments are shown in Supporting Information: Tables S1 and S2.

It can be seen in Figure 7 that the total impedance modulus obtained when the electrode was polarized at 0.8 V versus ref. in sulfuric acid was around 30 kΩcm^2. Different authors reported that anodized led yields a value between 15 and 60 kΩ. In any case, that value is highly dependent on the applied potential and polarization time. In general, the more anodizing the applied potential and polarization time, the higher the total impedance modulus will be.[33,54] The large total modulus obtained can be explained on the one hand by the compactness and thickness of the corrosion layer. On the second hand, it should be considered that the PbO formation in the corrosion layer becomes more dominant at anodic potentials (e.g., at 0.8 V vs. ref.). Then, because PbO is more resistive than $PbSO_4$,[55] it contributes to a large increase in the total modulus impedance. It is worth mentioning that Petiti et al. reported similar values with other compact products covering the metallic surface. In that case, the formation of a compact oxide layer on copper resulted in a large impedance value.[56] It can also be seen in the data fitting (see Supporting Information: Tables S1 and S2) that the equivalent circuit used for modeling the data was composed of a parallel combination of Rf1 and CPE1, representing the sulfate layer, in series with another parallel Rf2 and CPE2 combination, because of the presence of PbO in the corrosion layer. It is worth mentioning that large Rf1 and Rf2 values were obtained (25.8 and 4.9 kΩcm^2, respectively). These values proved the formation of a mixed corrosion layer composed of $PbSO_4$/PbO. In addition, the CPE1 (9.50 $\mu\Omega^{-1}s^n$) and CPE2 (4.37 $\mu\Omega^{-1}s^n$) values indicated that a compact corrosion layer was formed.[57–60] This fact is also proved by the surface micrography (Supporting Information: Figure S5) shown in the supplementary information.

A very different situation was obtained when the lead sample was exposed to vapors of acetic acid (see Figure 7). In that case, the obtained impedance modulus was around 6 kΩcm^2, which is much smaller than the value obtained in sulfuric acid (30 kΩcm^2). It is worth mentioning that a similar total impedance modulus are reported in copper when porous corrosion layers are formed on the metal surface.[61,62] In addition, when then the sample was exposed for 1 week to acetic acid, an *Rf* value of 4.54 kΩ cm^2 was obtained (see fitting data in Supporting Information: Table S1). This value is much smaller than the resistive values obtained with the sample anodized in sulfuric acid. These facts (total modulus and Rf value) were considered evidence of the high porosity of the corrosion layer and its lack of passivation. This result is also supported by the surface micrographs (Supporting Information: Figure S5).

At this point, EIS was used to evaluate the quality of the obtained surfaces after restoration using cold plasma.

Figure 8 shows the impedance spectra of a Pb surface before and after plasma restoration. The electrode was initially exposed to vapors of acetic acid for 1 week (as described in Section 2.2), and then, its corroded surface was restored using plasma conditions of experiment 7. Finally, to compare data to a reference value, the impedance spectrum of a noncorroded Pb electrode was also included in Figure 8. To perform the measurement, a Pb electrode was initially polished (see Section 2.3) and polarized at −1.4 V versus ref. in a 5 M H_2SO_4 solution for 1800 s. During polarization, the working electrode was rotated at 1500 rpm. Rotation of the working electrode was used to force the removal of hydrogen bubbles formed in the electrode surface during polarization. All fitting values are shown in Table 3. The fitting spectra of the sample restored by plasma and metallic lead were obtained using a Randles equivalent circuit.[21,53,63] Bode plots of the restored Pb surface by plasma treatment and metallic lead are shown in Supporting Information: Figures S8 and S9, respectively.

According to data shown in Table 3, the plasma-restored sample presented a residual corrosion layer ($Rf = 18.7\ \Omega\ cm^2$). It is also worth mentioning that the noncorroded lead electrode showed a similar resistive surface, yielding an *Rf* value of 12.4 Ωcm^2. Note that Karbasi et al. reported that pure Pb yields a resistance value of around 12 Ωcm^2.[64] In addition, Khatbi et al. reported similar values for lead-aluminum casting alloys for lead-acid batteries.[65] CPE values for both samples are in the same order of magnitude, due to similar dielectric properties of the residual layer formed on its surface. In any case, the total modulus obtained for the sample after plasma restoration (around 22 Ωcm^2) was much smaller than the value obtained for the sample before restoration (around 6 $k\Omega cm^2$). That fact indicates an important reduction of the resistive nature of the corrosion layer due to the plasma restoration process.

To analyze the composition of the residual corrosion layers after restoration, XRD analysis was performed (Figure 9) shows the obtained XRD spectra for the cold plasma treated sample with the parameters used for experiment 7 (see Table 1).

Figure 9 shows the superficial structural composition of each sample. In the cold plasma-treated sample, the presence of a thin layer composed mainly of PbO was confirmed after being analyzed by XRD. It means that a passive layer was

TABLE 3 Obtained results of the electron impedance spectroscopy resistances after the reduction of samples

	Metallic Pb	Plasma restored
Re (Ωcm^2)	1.35	1.85
Rf (Ωcm^2)	12.4	18.7
CPE ($\mu\Omega^{-1} cm^{-2} s^n$)	22	34.5
n	0.934	0.948

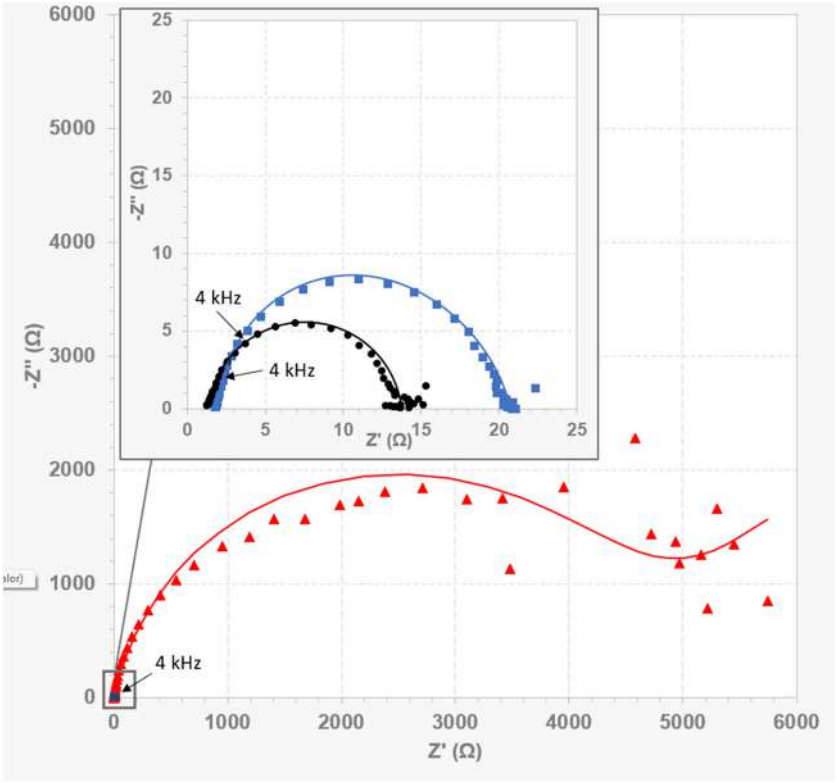

FIGURE 8 Electrochemical impedance spectroscopy spectra of the sample exposed one week to acetic acid (▲) and after being restored using hydrogen/argon (90:10) plasma at a potential of 50 W during 3600 s (■). EIS spectra of metallic Pb sample are also included (●).

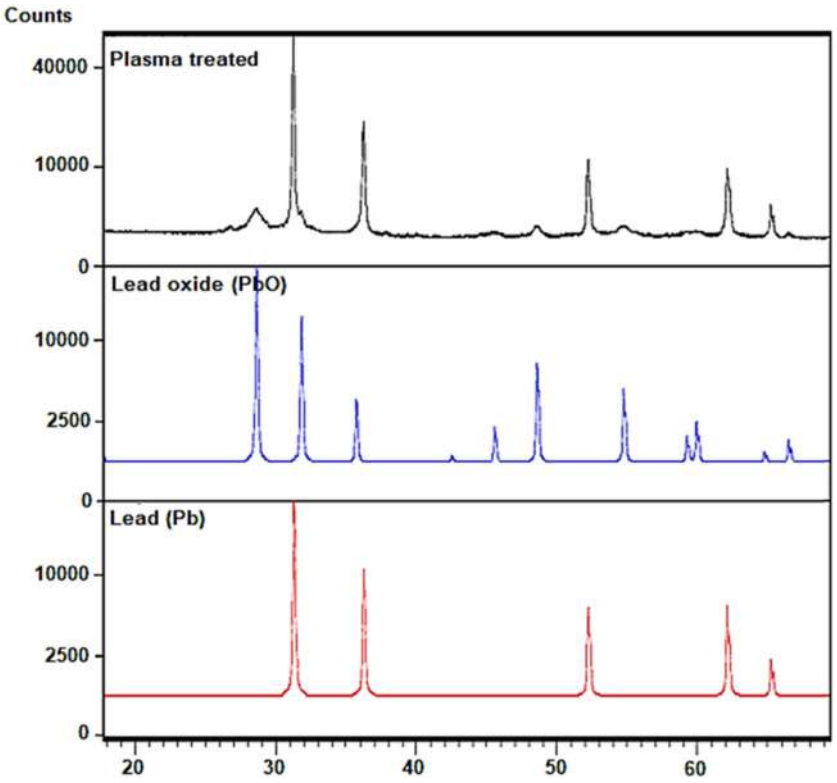

FIGURE 9 X-ray diffraction results after restoration; with cold plasma treatment conditions experiment 7

formed after the cold plasma restoration, and the lead carbonate proportion seen in the XPS analysis (seen in Figures 5 and 6) was very low. Note that EIS provided complementary information to XPS and XRD. In the present work, XPS was used to investigate the superficial chemistry of the samples, and XRD was used for phase identification of crystalline materials. In that frame, EIS provided additional information about the compactness, porosity, and thickness of these superficial layers.

At this point, it is worth mentioning that EIS is an analysis method commonly used for studies on understanding the fundamental processes of diffusion and faradaic reaction at electrodes. However, in the present work, it was used to evaluate the surface characteristics of corroded lead samples and also its potential to evaluate the quality of the restoration process. This fact is specifically relevant in the evaluation of corroded lead heritage artifacts because there is still a lack of consolidated protocols for their restoration, and very little information can be found in the bibliography.

In this work, it was demonstrated that when the lead is corroded and formed a stable, compact, and homogeneous layer (e.g., when lead was exposed to sulfuric acid environments), the obtained impedance spectra showed a large modulus, in the order of magnitude of $10^4\,\Omega cm^2$ or even larger. This fact indicates that despite the formation of a corroded film in the metal surface, the metal was protected against corrosion because of the compactness and stability of the corrosion layer. The corrosion layer blocked the access of the solvent to the metal, inhibiting its oxidation, and as a result, the specimen can be protected over long periods. In contrast, when porous and partially soluble corrosion products (e.g., when lead was exposed to acetic acid environments) formed, a smaller impedance modulus was obtained, in the order of magnitude of $10^3\,\Omega cm^2$. This fact indicates that the structural integrity of the sample may be at serious risk, and there should be a high concern for its conservation.

In the restoration of the Cultural Heritage field, surface characterization is the first approach to knowing the state of conservation of artifacts. This fact is critical when considering malleable metals such as lead. In this frame, techniques such as XRD, XPS, and SEM-EDS are frequently used in the field of restoration to characterize corroded surfaces. It should be noted that, in this field, EIS use is very infrequent. The present work demonstrated the potential of this technique to provide a fairly accurate analysis of its surface and it is presented as a useful and complementary tool to the classic techniques for surface analysis.

4 | CONCLUSIONS

The plasma technique is demonstrated to be useful for the restoration of ductile metals. Due to the low temperature used during the treatment, it was capable to restore corroded lead metals affected by acetic acid

environments, without damaging its structure. In this way, the cold plasma technique has been demonstrated to be a low-invasive methodology of restoration in comparison with traditional techniques. This treatment avoids the sample interaction with an electrolyte, preventing the introduction of new species. In addition, since plasma generates reactive species, the interaction between the particles and the surface is very efficient thanks to the fast kinetic. It allows for the restoration of the corroded surface in a shorter time than electrochemical reductions. It was proved that a combination of argon and hydrogen plasma increases the effectiveness of the treatment. Ionized argon induces the generation of reactive sites, increasing the efficiency of the hydrogen radicals during the plasma reduction.

In the present work, EIS was used to characterize corroded lead surfaces to determine the state of conservation. In addition, samples were also analyzed with EIS to evaluate the effectiveness of an argon/hydrogen cold plasma treatment in corroded surface restoration. Data obtained showed the potential of EIS to provide a fairly accurate analysis of the metal surface and also offer very useful information in the field of restoration, like the compactness and porosity of the corroded layers. Since there is still a lack of consolidated protocols for the restoration of malleable metals and very little information can be found in the bibliography, the presented work can be a complementary tool to the classical techniques for surface analysis.

The raw data required to reproduce these findings are available to download from https://www.dropbox.com/sh/82togl8ol2whset/AABR9cTtBVeRXp3kHsk180HZa?dl=0. The processed data required to reproduce these findings are available to download from https://www.dropbox.com/sh/82togl8ol2whset/AABR9cTtBVeRXp3kHsk180HZa?dl=0

DATA AVAILABILITY STATEMENT

Data is available on request from the authors.

ORCID

Sergi Colominas http://orcid.org/0000-0002-7678-2489
Salvador Borrós http://orcid.org/0000-0002-4003-0381

REFERENCES

[1] A. Crespo Ibañez, *Ge-Conservacion* **2019**, *16*, 327. https://doi.org/10.37558/gec.v16i0.720
[2] G. W. R. Ward, *Grove Encyclop. Mater. Tech. Art*, **2008**, 828. https://doi.org/10.1093/acref/9780195313918.001.0001
[3] A. V. Echavarria, F. E. Echeverria, C. Arroyave, E. Cano, J. M. Bastidas, *Corros. Rev.* **2003**, *21*, 395. https://doi.org/10.1515/CORRREV.2003.21.5-6.395
[4] E. R. Long, A. Bone, E. M. Breitung, D. Thickett, J. Grau-Bové, *Heritage Sci.* **2022**, *10*, 150. https://doi.org/10.1186/s40494-022-00778-3
[5] S. Msallamova, M. Kouril, K. C. Strachotova, J. Stoulil, K. Popova, P. Dvorakova, M. Lhotka, *Heritage Sci.* **2019**, *7*, 76. https://doi.org/10.1186/s40494-019-0317-3
[6] E. Mohammed, A. Adriaens, *Coatings* **2018**, *8*, 118. https://doi.org/10.3390/coatings8040118
[7] J. Švadlena, T. Prošek, T. Boháčková, M. Kouřil, *Koroze Ochr. Mater.* **2021**, *65*, 1. https://doi.org/10.2478/kom-2021-0013
[8] A. Towarek, A. Mistewicz, E. Pilecka-pietrusińska, J. Zdunek, J. Mizera, *J. Archaeol. Sci. Rep.* **2022**, *45*, 103611. https://doi.org/10.1016/j.jasrep.2022.103611
[9] E. R. Caley, *Stud. Conserv.* **1955**, *2*, 49. https://doi.org/10.2307/1504917
[10] M. Gilberg, *J. Am. Instit. Conservat.* **1987**, *26*, 105. https://doi.org/10.1179/019713687806027843
[11] O. Schalm, P. Storme, A. Gambirasi, M. Favaro, A. Patelli, *Surf. Interface Anal.* **2018**, *50*, 32. https://doi.org/10.1002/sia.6329
[12] A. Patelli, E. Verga, L. Nodari, S. M. Petrillo, A. Delva, P. Ugo, P. Scopece, *IOP Conf. Series Mater. Sci. Eng.* **2018**, *364*, 012079. https://doi.org/10.1088/1757-899X/364/1/012079
[13] R. Tiňo, K. Vizárová, F. Krčma, *Nanotechnologies and Nanomaterials for Diagnostic, Conservation and Restoration of Cultural Heritage*, Elsevier, **2019**, pp. 239. https://doi.org/10.1016/B978-0-12-813910-3.00011-2
[14] M. J. A. Salvador Borrós Gómez, L. Robbiola, J. Esteve, M. Pugès, *Revista de Química Teórica y Aplicada* **2005**, *62*, 513.
[15] N. A. Salvador Borrós Gómez, *La Técnica de Plasma de frío Como Herramienta en Restauración y Conservación de Material Arqueológico*. Innovación Tecnológica En Conservación y Restauración Del Patrimonio, **2006**: pp. 64–73.
[16] S. B. G. J. Esteve, M. Alonso, *Método Para la Restauración de Planchas Calcográficas de cinc Mediante la Técnica de Plasma Frío*, Revista de Arte, Goya **2001**, 308.
[17] L. La-Torre-Riveros, A. Doménech-Carbó, C. R. Cabrera, M. T. Doménech-Carbó, W. Huahuasoncco-Condori, D. Quispe Guzmán, M. C. Gutiérrez-Castillo, K. Carmona-Ochoa, A. Pérez-Trujillo, *J. Solid State Electrochem.* **2019**, *23*, 1541. https://doi.org/10.1007/s10008-019-04243-3
[18] E. Apchain, D. Neff, J.-P. Gallien, N. Nuns, P. Berger, A. Noumowé, P. Dillmann, *Corros. Sci.* **2021**, *183*, 109319. https://doi.org/10.1016/j.corsci.2021.109319
[19] Valentini, *Smart Electrochemical Portable Tools for Cultural Heritage Analysis: A Review, Sensors* **2019**, *19*, 4303. https://doi.org/10.3390/s19194303
[20] D. Mikić, H. Otmačić Ćurković, T. Kosec, N. Peko, *Materials* **2021**, *14*, 2063. https://doi.org/10.3390/ma14082063
[21] F. di Turo, P. Matricardi, C. di Meo, F. Mazzei, G. Favero, D. Zane, *J. Cult. Herit.* **2019**, *37*, 113. https://doi.org/10.1016/j.culher.2018.09.017
[22] J. C. Aguilar, D. E. Arceo-Gómez, M. A. Hernandez-Perez, R. Galvan-Martinez, R. Orozco-Cruz, *ECS Trans.* **2019**, *94*, 345. https://doi.org/10.1149/09401.0345ecst
[23] L. Iannucci, J. F. Ríos-Rojas, E. Angelini, M. Parvis, S. Grassini, *Eur. Phys. J. Plus* **2018**, *133*, 522. https://doi.org/10.1140/epjp/i2018-12368-3
[24] L. E. Sebar, E. Angelini, S. Grassini, L. Iannucci, M. Parvis, *An op amp-less Electrochemical Impedance Spectroscopy System*. 2020 IEEE International Instrumentation and Measurement Technology Conference (I2MTC), IEEE; **2020**. 1–6. https://doi.org/10.1109/I2MTC43012.2020.9129355

[25] D. Arguelles, C. Campechano, R. Galván-Martínez, T. Jimenez, R. Orozco-Cruz, *ECS Meet. Abstr.* **2018**, *MA2018-02*, 2072. https://doi.org/10.1149/MA2018-02/58/2072
[26] C. Petiti, L. Toniolo, D. Gulotta, B. Mariani, S. Goidanich, *Environ. Sci. Pollut. Res.* **2020**, *27*, 13081. https://doi.org/10.1007/s11356-020-07814-4
[27] L. E. Sebar, L. Iannucci, E. Angelini, S. Grassini, M. Parvis, *IEEE Trans. Instrum. Meas.* **2021**, *70*, 1. https://doi.org/10.1109/TIM.2020.3038005
[28] A. Bogaerts, R. Gijbels, *J. Anal. Spectrom.* **2000**, *15*, 1191. https://doi.org/10.1039/b000519n
[29] A. Patelli, E. Verga, L. Nodari, S. M. Petrillo, A. Delva, P. Ugo, P. Scopece, *IOP Conf. Series Mater. Sci. Eng.* **2018**, *364*, 012079. https://doi.org/10.1088/1757-899X/364/1/012079
[30] T. Makabe, *Atom. Mole. Opt. Phys.* **2001**, *44*, 127. https://doi.org/10.1016/S1049-250X(01)80031-8
[31] B. Ramírez Barat, E. Cano, *ChemElectroChem* **2018**, *5*, 2698. https://doi.org/10.1002/celc.201800844
[32] E. Cano, D. Lafuente, D. M. Bastidas, *J. Solid State Electrochem.* **2010**, *14*, 381. https://doi.org/10.1007/s10008-009-0902-6
[33] M. M. Burashnikova, I. A. Kazarinov, I. V. Zotova, *J. Power Sources* **2012**, *207*, 19. https://doi.org/10.1016/j.jpowsour.2011.12.042
[34] Y.-Y. Wang, K. Kusumoto, C.-J. Li, *Phys. Procedia* **2012**, *32*, 95. https://doi.org/10.1016/j.phpro.2012.03.524
[35] J. Xu, X. Li, X. Liu, N. Deem, E. Barbero, C. Dong, *Metallurg. Mater. Trans. A* **2005**, *36*, 2175. https://doi.org/10.1007/s11661-005-0337-3
[36] B. Strohmeier, R. White, T. Nunney, P. Mack, A. Wright, *Microsc. Microanal.* **2014**, *20*, 2062. https://doi.org/10.1017/S1431927614012045
[37] P. Mattesco, N. Bui, P. Simon, L. Albert, *J. Power Sources* **1997**, *64*, 21. https://doi.org/10.1016/S0378-7753(96)02495-0
[38] K. C. Sabat, P. Rajput, R. K. Paramguru, B. Bhoi, B. K. Mishra, *Plasma Chem. Plasma Process.* **2014**, *34*, 1. https://doi.org/10.1007/s11090-013-9484-2
[39] J. W. Coburn, H. F. Winters, *J. Vac. Sci. Technol.* **1979**, *16*, 391. https://doi.org/10.1116/1.569958
[40] V. M. Donnelly, A. Kornblit, *J. Vac. Sci. Technol. A* **2013**, *31*, 0508251. https://doi.org/10.1116/1.4819316
[41] R. Tiňo, K. Vizárová, F. Krčma, *Adv. Nanomater.* **2019**, 239. https://doi.org/10.1016/B978-0-12-813910-3.00011-2
[42] R. A. Gottscho, *J. Vacu. Sci. Technol. Microelectron. Nanom. Struct.* **1992**, *10*, 2133. https://doi.org/10.1116/1.586180
[43] K. Schmidt-Ott, V. Boissonnas, *Stud. Conserv.* **2002**, *47*, 81. https://doi.org/10.1179/sic.2002.47.2.81
[44] A. V. Naumkin, A. K. raut-Vass, S. W. Gaarenstroom, C. J. PowellNIST X-ray Photoelectron Spectroscopy Database. NIST Standard Reference Database 20, Version 4.1; **2000**.
[45] D. Briggs, *Surf. Interface Anal.* **1981**, *3*, 199. https://doi.org/10.1002/sia.740030412
[46] P. S. de Velasco Maldonado, V. Hernández-Montoya, A. Concheso, M. A. Montes-Morán, *Appl. Surf. Sci.* **2016**, *386*, 381. https://doi.org/10.1016/j.apsusc.2016.06.025
[47] A. Coccato, L. Moens, P. Vandenabeele, *Heritage Sci.* **2017**, *5*, 12. https://doi.org/10.1186/s40494-017-0125-6
[48] D. Pavlov, *J. Power Sources* **2004**, *137*, 288. https://doi.org/10.1016/j.jpowsour.2004.06.006
[49] J. Tétreault, J. Sirois, E. Stamatopoulou, *Stud. Conserv.* **1998**, *43*, 17. https://doi.org/10.1179/sic.1998.43.1.17
[50] P. Simon, N. Bui, N. Pebere, F. Dabosi, L. Albert, *J. Power Sources* **1995**, *55*, 63. https://doi.org/10.1016/0378-7753(94)02175-3
[51] J. Yu, Z. Qian, M. Zhao, Y. Wang, L. Niu, *Chem. Res. Chin. Univ.* **2013**, *29*, 374. https://doi.org/10.1007/s40242-013-2261-1
[52] P.-Y. Zhang, Z.-L. Liu, *J. Power Sources* **2010**, *195*, 8013. https://doi.org/10.1016/j.jpowsour.2010.06.062
[53] A. R. C. Bredar, A. L. Chown, A. R. Burton, B. H. Farnum, *ACS Appl. Energy Mater.* **2020**, *3*, 66. https://doi.org/10.1021/acsaem.9b01965
[54] F. E. Varela, L. M. Gassa, J. R. Vilche, *J. Electroanal. Chem.* **1993**, *353*, 147. https://doi.org/10.1016/0022-0728(93)80293-Q
[55] R. Brinic, M. Metkos-Hukovic, S. Babic, *J. New Mater. Electrochem. Syst.* **2005**, *8*(4), 273.
[56] C. Petiti, D. Gulotta, B. Mariani, L. Toniolo, S. Goidanich, *J. Solid State Electrochem.* **2020**, *24*, 3257. https://doi.org/10.1007/s10008-020-04822-9
[57] D. Pavlov, P. Nikolov, *J. Electrochem. Soc.* **2012**, *159*, A1215. https://doi.org/10.1149/2.035208jes
[58] S. A. A. Sajadi, *Am. J. Anal. Chem.* **2011**, *02*, 206. https://doi.org/10.4236/ajac.2011.22024
[59] Y. Guo, L. Niu, S. Zhang, S. Chen, *J. Power Sources* **2000**, *85*, 38. https://doi.org/10.1016/S0378-7753(99)00379-1
[60] P. Gao, Y. Liu, W. Lv, R. Zhang, W. Liu, X. Bu, G. Li, L. Lei, *J. Power Sources* **2014**, *265*, 192. https://doi.org/10.1016/j.jpowsour.2014.04.045
[61] I. Martinović, Z. Pilić, *Mater. Corros.* **2021**, *72*, 1635. https://doi.org/10.1002/maco.202112470
[62] F. Deflorian, M. Fedel, *J. Cult. Herit.* **2013**, *14*, 254. https://doi.org/10.1016/j.culher.2012.06.002
[63] P. Letardi, *Corros. Conservat. Cult. Heritage Metallic Artef.* **2013**, 126. https://doi.org/10.1533/9781782421573.2.126
[64] M. Karbasi, E. Keshavarz Alamdari, E. Amirkhani Dehkordi, F. Tavangarian, *J. Appl. Electrochem.* **2018**, *48*, 379. https://doi.org/10.1007/s10800-018-1163-9
[65] S. Khatbi, Y. Gouale, S. Mansour, A. Lamiri, M. Essahli, *Port. Electrochim. Acta* **2018**, *36*, 133. https://doi.org/10.4152/pea.201802133

SUPPORTING INFORMATION

Additional supporting information can be found online in the Supporting Information section at the end of this article.

How to cite this article: P. Giménez-Barrera, S. Colominas, S. Borrós, *Plasma Processes Polym.* **2023**;20:e2200136. https://doi.org/10.1002/ppap.202200136